Received: 28 November 2017 | Revised: 23 April 2018 | Accepted: 24 April 2018

DOI: 10.1002/jrs.5399

RESEARCH ARTICLE

WILEY Journal of RAMAN SPECTROSCOPY

An adaptive denoising method for Raman spectroscopy based on lifting wavelet transform

Hao Chen[1,2] | Weiliang Xu[1,2] | Neil Broderick[2,3] | Jianda Han[4,5]

[1]Department of Mechanical Engineering, The University of Auckland, Auckland, New Zealand

[2]The Dodd-Walls Center for Photonic and Quantum Technologies, Auckland, New Zealand

[3]Department of Physics, The University of Auckland, Auckland, New Zealand

[4]College of Computer and Control Engineering, Nankai University, Tianjin, China

[5]State Key Lab of Robotics, Shenyang Institute of Automation, Chinese Academy of Sciences, Shenyang, China

Correspondence
Weiliang Xu, Department of Mechanical Engineering, The University of Auckland, Auckland, New Zealand.
Email: p.xu@auckland.ac.nz

Abstract

Noise, especially high-level noise, is a severe problem in Raman spectral analysis. It smears informative Raman peaks, distorts spectral features, and therefore affects final analytical results, particularly in multivariate analysis, which is frequently used in Raman spectroscopy. This becomes even worse when it comes to optical Raman probe-based biological applications due to limited acquisition time, laser power, and collection efficiency. Noise suppression is usually the first step in the preprocessing procedure of Raman spectral analysis. It is crucial to reduce noise effectively before performing further analysis. Discrete wavelet transform is a useful tool for noise reduction. However, it only provides limited and fixed filter banks, which may not be optimal for the data under investigation. In this paper, a novel adaptive denoising method based on lifting wavelet transform is presented for improving the signal-to-noise ratio for a Raman probe-based system. It enables users to develop an infinite number of lifting schemes from a base wavelet, and with the help of genetic algorithm, the optimal one can be easily found. This method is examined by a set of simulated Raman spectra with various noise level and a set of experimental Raman spectra. Performance comparison with other commonly used denoising methods is made. The results indicate that the proposed method is able to remove noise effectively while retaining informative Raman peaks satisfactorily.

KEYWORDS

adaptive denoising, lifting wavelet transform, noise reduction, Raman spectroscopy

1 | INTRODUCTION

Over the past a few decades, Raman spectroscopy has been widely used as a powerful and promising technique in various fields including analytical chemistry and biomedical applications. It is an optical technique that utilizes inelastic scattering photons to probe the vibrational modes of chemical bonds of samples. Raman spectroscopy is able to analyze samples on a molecular level and provide its "fingerprint" spectral features. However, the process of Raman scattering effect is intrinsically weak. Typically, only 1 in 10^6 to 10^8 photons will experience Raman scattering effect.[1]

Noise is pervasive in any type of measurement data, and generally, it can be ignored due to high signal-to-noise ratio (SNR). But when it comes to Raman spectra, because of the weakness of Raman effects and low intensity of Raman peaks, simply neglecting the influence of noise will pose a negative impact on further analysis of the Raman spectral data, for example, affecting the accuracy of a classification model for cancer diagnosis. The best way to suppress noise is to use highly sensitive and stable instruments

and conduct spectral measurement under optimal experimental conditions. However, these conditions cannot always be met due to either instrumental limitations or application constraints. For Raman probe-based in vivo applications, because of limited integration time and laser power to avoid phototoxicity and photodamage to the sample, the SNR of the acquired spectra is much lower than spectra taken through Raman micro-spectroscopy. Thus, additional noise removal steps need to be performed before further analysis on the spectral data.

Various types of noise can be recognized in the process of Raman spectra acquisition, for example, noise due to dark current and read noise (generated by analog-digital convertor in the spectrometer). In a measured Raman spectrum, fluorescence background noise and random noise are the two major types of noise. In this paper, we only focus on the random noise reduction. The fluorescence background, which may be very strong especially for biological samples, can be effectively removed using various methods, such as methods based on polynomial fitting,[2,3] least square,[4,5] or first derivate.[6,7] The random noise is a high-frequency component compared with Raman peaks and low-frequency background, and its intensity is highly dependent on the equipment and measurement condition. The commonly used method for random noise reduction is smoothing. Among different smoothing techniques, first order or second order Savitzky–Golay (SG) filter is a widely used one.[8] Like most smoothing techniques, an SG filter smooths a Raman spectrum in the whole range, and Raman peaks are also affected. It is obvious that improvements on noise treatment are still required.

Discrete wavelet transform (DWT) solves the fluorescence background and random noise problem by decomposing the original spectrum into a series of wavelet (detail) coefficients and scale (approximation) coefficients, which are both time and frequency features of raw data. Usually, random noise has the highest frequency in the spectrum, whereas informative Raman peaks have a moderate frequency, and the fluorescence background has the lowest frequency. So DWT is able to separate these three components and process noise and background while retaining Raman features.[9–11] However, conventional DWT applies fixed filter banks normally choosing from the standard types of wavelets, which results in a suboptimal solution for the spectral data.[12,13] A better result can be achieved by designing and constructing an adaptive wavelet filter according to the characteristics of experiment data being studied.

In this work, an adaptive lifting wavelet transform (ALWT) denoising method for random noise reduction in Raman spectroscopy is proposed. ALWT allows users to develop an infinite number of lifting schemes from the lifting scheme of a chosen base wavelet. Genetic algorithm (GA) is applied to search for the optimal one that suits the data at hand best. This method requires no prior knowledge about background information and chemical composition of the sample. Besides, it can also be applied to other vibrational spectroscopies. In order to evaluate the performance of this method, three simulated spectra with various noise level and a set of experimental Raman spectrum are used. The results prove the effectiveness of the proposed method.

2 | ADAPTIVE LIFTING WAVELET TRANSFORM

2.1 | Principal of lifting scheme

In 1998, Sweldens proposed the method on constructing second generation wavelet based on lifting scheme.[14] Unlike conventional wavelet transform, lifting wavelet transform (LWT) avoids the Fourier transform completely and does not rely on scaling and translating operations of base wavelet. LWT is highly efficient, fast in calculation speed, requires little memory, and it inherits all of the great properties of conventional DWT. It designs suitable wavelet filters and uses them to perform wavelet transform. A typical lifting scheme is composed of iteration operations of three steps: split, predict, and update. Suppose a_i is the approximation coefficients at the ith decomposition level, the three steps are depicted as follows:

(1) Split: a_i is divided into two disjoint subsets. A frequently used method is lazy wavelet transform (Equation 1), which extracts odd-indexed (a_i^{odd}) and even-indexed data points (a_i^{even}).The z-transform of lazy wavelet transform is shown in Figure 1. Other data division methods can also be applied.

$$\begin{cases} a_i^{odd}(k) = a_i(2k-1) \\ a_i^{even}(k) = a_i(2k) \end{cases}, k = 1,\ 2\ ...,\ \text{length}(a_i)/2. \quad (1)$$

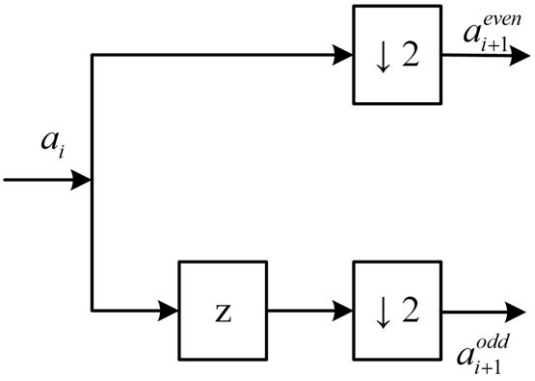

FIGURE 1 Illustration of lazy wavelet transform (z represents the unit advance operator and ↓2 denotes downsampling by two)

(2) Predict (dual lifting): in this operation, the odd subset a_i^{odd} is predicted by a linear combination (also known as prediction operator, denoted as P) of several neighboring even samples. The odd subset a_i^{odd} is then replaced by the difference between a_i^{odd} and the predicted value, and it becomes the detail or wavelet coefficients at $i + 1$th level, d_{i+1}:

$$d_{i+1} = a_{i+1}^{odd} - P\left(a_{i+1}^{even}\right). \tag{2}$$

(3) Update (primal lifting): in this step, the even subset a_{i+1}^{even} is updated based on detail coefficients d_{i+1} by an updating operator U:

$$a_{i+1} = a_{i+1}^{even} + U(d_{i+1}). \tag{3}$$

These three steps iterated until the highest decomposition level is reached. The inverse LWT is symmetrical to the above process and has three counter steps:

(1) Update:

$$a_{i+1}^{even} = a_{i+1} - U(d_{i+1}). \tag{4}$$

(2) Predict:

$$a_{i+1}^{odd} = d_{i+1} + P\left(a_{i+1}^{even}\right). \tag{5}$$

(3) Merge:

$$a_i = \text{Merge}\left(a_{i+1}^{odd}, a_{i+1}^{even}\right). \tag{6}$$

The process of LWT and inverse LWT is illustrated in Figure 2.

2.2 | Adaptive lifting wavelet transform

Instead of designing the prediction and update operators from the beginning, an easier way to design the desired wavelet is to modify an existing one whose properties are well recognized and is suitable to generate a second generation wavelet. Daubechies and Sweldens demonstrated that any wavelet transform with finite impulse response filters can be decomposed into a finite number of lifting steps.[15] As mentioned above, dual lifting and primal lifting are the two main lifting strategies of LWT. Detail coefficients are obtained by lifting the performance of high-pass filter with the help of low-pass sub-band, whereas approximation coefficients are obtained by lifting the performance of low-pass filter with the help of high-pass sub-band. By adding one or several elementary lifting steps (ELSs), we can generate an infinite number of second generation wavelets from a selected base wavelet. Finding an optimal one to best suit the spectral data at hand, desired denoising result could be obtained. As noise has a higher frequency compared with Raman features, we only use primal lifting to better retain low-frequency approximation coefficients in ALWT. To further simplify the calculation complexity, an additional one-step primal lifting based on a selected base wavelet is adopted in this work.

The main procedure of the proposed method is given as follows:

(1) Choose a base wavelet with finite impulse response quadruplet filters that satisfies perfect reconstruction conditions[15]:

$$\begin{aligned} h_r(z)h_d\left(z^{-1}\right) + g_r(z)g_d\left(z^{-1}\right) &= 2 \\ h_r(z)h_d(-z^{-1}) + g_r(z)g_d(-z^{-1}) &= 0, \end{aligned} \tag{7}$$

where the decomposition filters are denoted as h_d (low-pass filter) and g_d (high-pass filter), the reconstruction filters are denoted as h_r (low-pass filter) and g_r (high-pass filter), and $h_r(z)$, $g_r(z)$, $h_d(z^{-1})$, $g_d(z^{-1})$ are their corresponding z-transform forms. Many wavelets from the eight standard types of wavelets can satisfy the above requirements. Here, we choose Daubechies 4 wavelet (db4) as the base wavelet. Although somewhat arbitrary, it turns out to be suitable for the data we use in this paper. For a classification problem with a large dataset, a supervised ALWT on the whole or a subset of

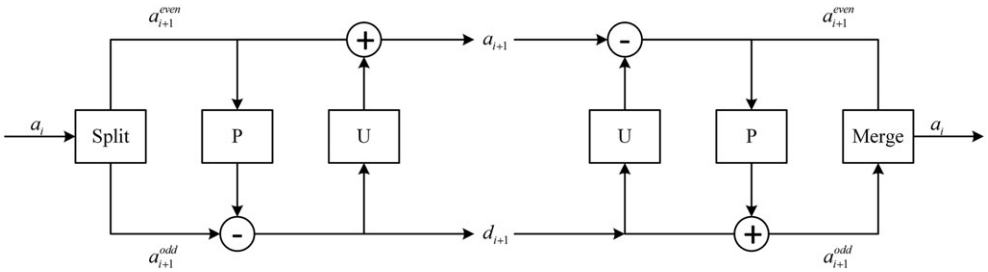

FIGURE 2 A schematic diagram of lifting wavelet transform and inverse lifting wavelet transform

calibration set would serve better in selecting the suitable base wavelet.

(2) Construct the polyphase matrix $\boldsymbol{P}$, which is associated with the quadruplets using the reconstruction filters h_r and g_r. The polyphase matrix is of the following form:

$$\boldsymbol{P}(z) = \begin{bmatrix} h_r^{even}(z) & g_r^{even}(z) \\ h_r^{odd}(z) & g_r^{odd}(z) \end{bmatrix}, \tag{8}$$

where h_r^{even} and g_r^{even} are the even terms of $h_r(z)$ and $g_r(z)$, and h_r^{odd} and g_r^{odd} are the odd terms of $h_r(z)$ and$g_r(z)$. And they can be calculated by

$$f^{even}(z^2) = (f(z) + f(-z))/2$$
$$f^{odd}(z^2) = (f(z) - f(-z))/2z^{-1}.$$

(3) Factor the polyphase matrix using the Euclidean factoring algorithm.[15] $\boldsymbol{P}$ can be factored into

$$\boldsymbol{P}(z) = \prod_{i=1}^{m} \begin{bmatrix} 1 & s_i(z) \\ 0 & 1 \end{bmatrix} \begin{bmatrix} 1 & 0 \\ t_i(z) & 1 \end{bmatrix} \begin{bmatrix} K & 0 \\ 0 & 1/K \end{bmatrix}, \tag{9}$$

where $\begin{bmatrix} 1 & s_i(z) \\ 0 & 1 \end{bmatrix}$ is related to a primal lifting step and $\begin{bmatrix} 1 & 0 \\ t_i(z) & 1 \end{bmatrix}$ is related to a dual lifting step, K is a scaling factor decided by the factoring algorithm to ensure perfect reconstruction, and $s_i(z)$ and $t_i(z)$ are Laurent polynomials with the following form:

$$f(z) = f_1 z^{\max} + f_2 z^{\max-1} + \ldots + f_{end} z^{\min}, \tag{10}$$

where max is the highest degree, min is the lowest degree of $f(z)$, andmax − min defines the length of $f(z)$.

(4) The lifting scheme LS of the base wavelet then can be obtained from the factorization of $\boldsymbol{P}(z)$. It consists of a sequence of primal and dual ELSs.

(5) Add an optimal primal ELS to the lifting scheme LS to obtain an improved new lifting scheme, LSN. With proper parameters, LSN is expected to be more suitable to the spectral data at hand than LS. This optimal primal ELS and the most suitable decomposition level j are obtained through multi-objective GA searching with a given length of a Laurent polynomial. Other optimization algorithms may also work, but GA has its own advantages. Unlike other traditional optimization methods, GA searches parallel from a population of starting points thus avoiding being trapped in local optimal solutions. It is also suitable for noisy objective functions and searching multiple objectives. The input (a vector) of the multi-objective GA searching consists of three major parts: the decomposition level, the coefficients of a Laurent polynomial of ELS, and the maximum degree of this Laurent polynomial. The detailed parameter settings of GA searching are given in Table 2, and the two searching objectives are given in Section 2.3. GA searching finds the optimal input by searching the optimal values of the two objectives.

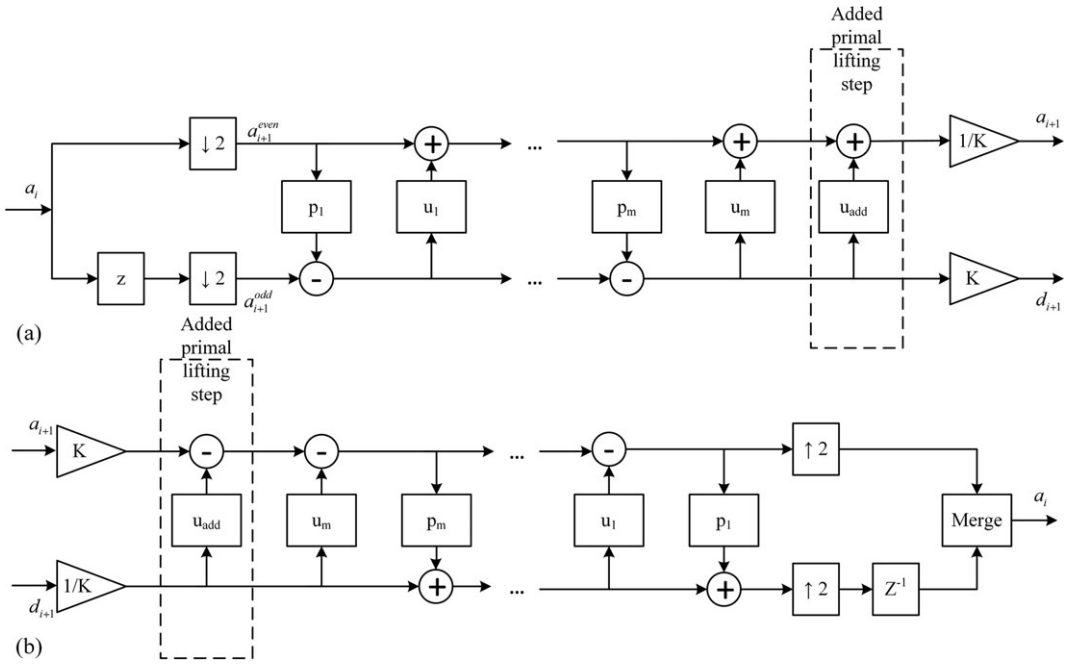

FIGURE 3 Forward and inverse implementations of adaptive lifting wavelet transform (ALWT): (a) forward ALWT; (b) inverse ALWT

(6) Perform ALWT on the input spectrum x using LSN. The ALWT process is illustrated in Figure 3a. First, implementing lazy wavelet transform, then performing primal and dual lifting steps in LS and the added primal ELS, finally a scaling by factor K. The additional primal ELS u_{add} is shown in the dashed box, other parts except the dashed box all belong to LS.

(7) Process the detail coefficients with certain threshold value. Choosing a suitable threshold value is of great importance in the wavelet denoising procedure. A popular threshold selection method, the "universal" threshold method,[16] is adopted in this paper. The universal threshold λ is defined as

$$\lambda = \frac{median(d)}{0.6745}\sqrt{2\log N}, \tag{11}$$

where d is a vector of detail coefficients, $median(\cdot)$ is the median value function, and N is the length of d.

Two main strategies used for suppressing the detail coefficients are soft thresholding and hard thresholding. Hard thresholding can better preserve local characteristics and sudden changes of the input signal; however, it suffers from the pseudo-Gibbs phenomena due to the discontinuities at $\pm\lambda$. Soft thresholding can give a relatively smooth results and can moderate the pseudo-Gibbs effect. Therefore, the soft thresholding strategy is applied.

(8) Inverse ALWT to reconstruct the signal after noise reduction. Figure 3b shows the inverse ALWT process.

The flowchart of ALWT denoising algorithm is shown in Figure 4.

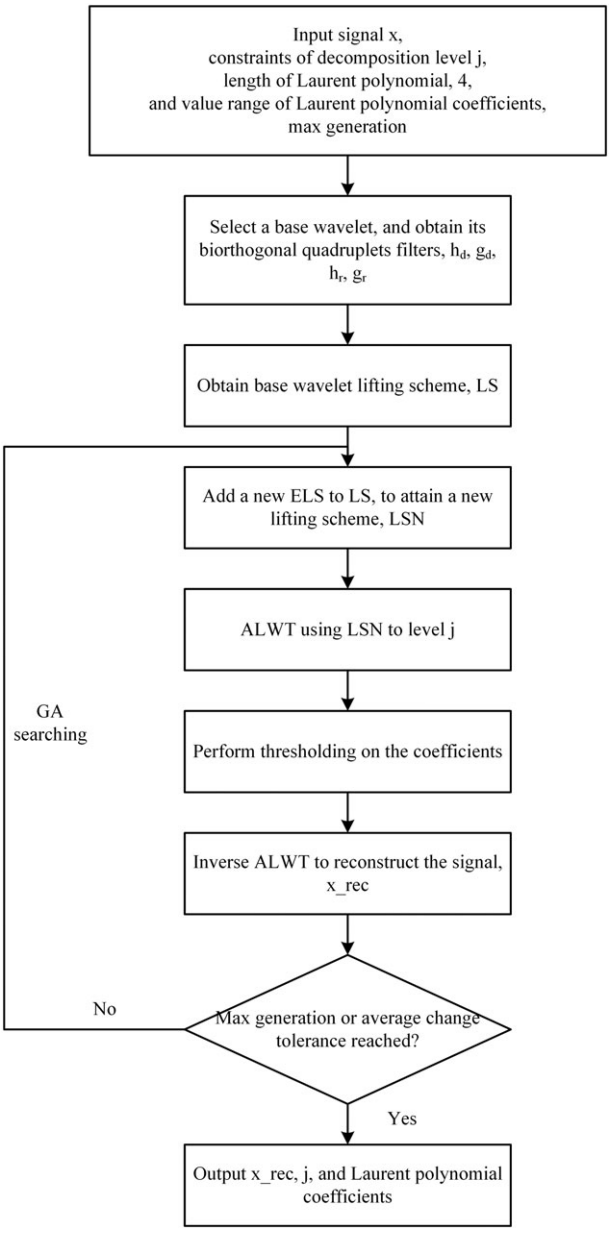

FIGURE 4 Flowchart of adaptive lifting wavelet transform (ALWT) denoising. GA = genetic algorithm; ELS = elementary lifting step

2.3 | Evaluation criteria

To evaluate the performance of the proposed denoising method and make comparison with other commonly used denoising methods in Raman spectroscopy, two indices are introduced as performance assessment criteria: the estimated signal-to-noise ratio (eSNR) after reconstruction and root mean square error (RMSE). These two indices are also used as the objectives for GA searching.

$$eSNR = 10\lg\left\{\frac{\sum_{i=0}^{N-1} x\_rec_i^2}{\sum_{i=1}^{N-1}(x_i - x\_rec_i)^2}\right\}, \tag{12}$$

$$RMSE = \sqrt{\frac{1}{N}\sum_{i=1}^{N}(x_i - x\_rec_i)^2}, \tag{13}$$

where x_i is the raw spectrum and x_rec_i is the reconstructed spectrum.

3 | SIMULATED AND EXPERIMENTAL SPECTRA

Two types of Raman spectra were examined: three simulated Raman spectra with various noise level and a set of real Raman spectra taken from swine fatty tissue.

Comparison was made between the proposed denoising method and commonly used methods, that is, first, second, and third order SG filters, and wavelet transform using the same base wavelet without additional lifting.

The Matlab 2017b (The MathWorks Inc., USA) equipped with wavelet toolbox version 4.15 and optimization toolbox version 7.3 runs under the operating system Microsoft Windows 7 Professional was used to develop the algorithm.

3.1 | Generation of simulated spectra

A measured Raman spectrum usually consists of three major components: Raman peaks $\boldsymbol{y_r}$, fluorescence background $\boldsymbol{b}$, and random noise $\boldsymbol{n}$. So a Raman spectrum can be expressed as $\boldsymbol{y} = \boldsymbol{y_r} + \boldsymbol{b} + \boldsymbol{n}$. The simulated Raman peaks are produced by the sum of a sequence of Lorentzian peaks, via

$$\boldsymbol{y_r} = \sum_{i=1}^{m} \frac{2A_i}{\pi} \frac{w_i}{4(x-x_i)^2 + w_i^2}, \tag{14}$$

where m is the total number of peaks, A_i is the area under curve from baseline, w_i is the parameter related to the peak width, and x_i is the peak position along horizontal axis. Parameters used for generating Raman peaks are provided in Table 1.

The fluorescence background $\boldsymbol{b}$ was then simulated by a fourth order polynomial. The shape was chosen to mimic fluorescence in biological samples. Gaussian white noise was then added to the simulated signal with amplitudes of 10%, 20%, and 30% of the lowest Raman peak. The three simulated spectra $\boldsymbol{y}_1$, $\boldsymbol{y}_2$, and $\boldsymbol{y}_3$ were constructed in the range of 200 to 1,800 cm^{-1} and shown in Figure 5.

3.2 | Experimental spectra

Experimental Raman spectra of swine fatty tissue were obtained using a portable fiber-optic Raman sensing system. This system consists of a 785-nm continuous laser source (FC-D-785, X2 Labwares Private Limited, Singapore), a fiber-optic Raman probe (EmVison LLC, FL, USA), a compact spectrometer (TG-Raman 785–1,100 nm, X2 Labwares Private Limited), and a computer. The swine fatty tissue sample for human consumption was purchased from supermarket. Three spectra using different laser power (90, 60, and 30 mW at the sample, respectively) with 1-s integration time for each spectrum were taken to imitate various noise levels in simulated spectra. Here, we denote the three spectra as $\mathbf{s_1}$, $\mathbf{s_2}$, and $\mathbf{s_3}$, respectively.

3.3 | Classification dataset

To illustrate the performance of the proposed method on a classification problem, a bladder tissue spectral dataset that was obtained previously using the same instruments described above ex vivo was included in this study. Laser power at sample was around 40 mW. Briefly, this dataset contains 136 bladder tumor spectra and 88 normal bladder spectra. The dataset was first denoised using the above mentioned noise reduction methods, and then, same preprocessing procedures including baseline correction and standard normal variate were applied. Principal

TABLE 1 Parameters used for simulated Raman peaks

x_i	A_i	w_i
623	89	20
801	96	15
946	78	10
1,001	35	6
1,024	57	10
1,086	105	33
1,128	70	74
1,260	180	22
1,288	90	24
1,322	88	22
1,348	130	17
1,460	188	13
1,652	160	28

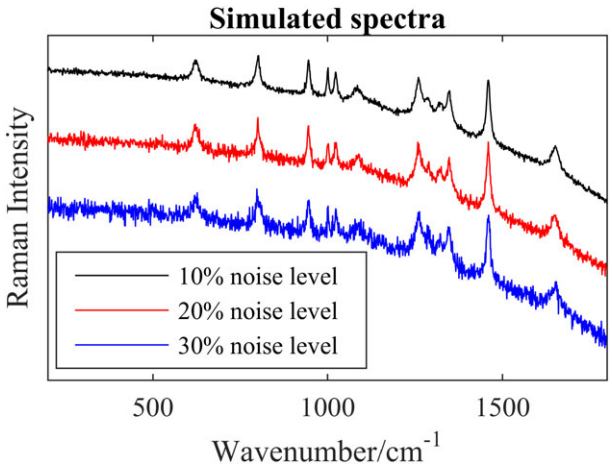

FIGURE 5 Simulated spectra with various noise level, 10% (black line), 20% (red line), and 30% (blue line) of the generated lowest Raman peak (offset for visualization) [Colour figure can be viewed at wileyonlinelibrary.com]

component analysis (PCA) was then applied on the preprocessed data and principal components that can accumulatively explain over 90% variance of the spectral data were fed into a linear discriminant analysis (LDA) model with 10-fold cross-validation.

4 | RESULTS AND DISCUSSION

4.1 | Simulated spectra

Because random noise reduction is the major focus of this method, the background $\boldsymbol{b}$ was considered as a part of useful signal and was reconstructed. The denoising procedure described in Figure 4 was applied on the simulated spectra, and the relevant parameter settings used in the multi-objective GA searching are listed in Table 2. The searching objectives are the two performance evaluation criteria. The decomposition level j was set within the range of [1, 10] to ensure enough data points in the approximation and wavelet coefficients at the highest decomposition level. Usually, the highest decomposition level should be less than $\log_2 N$ (where N is the signal length). After dozens of trials of GA searching on the simulated spectra, the coefficients of Laurent polynomial used in the added ELS always fell in the range [−2, 2]. So [−2, 2] was set as the searching range of Laurent polynomial coefficients for simplicity. A better result is anticipated when a wider range is selected, especially for unknown data. And the range of maximum degree of Laurent polynomial was also decided empirically.

After performing the multi-objective GA searching, the optimal parameters were found for the three simulated spectra. To eliminate undesired fluctuations generated at both ends, the reconstructed spectra were truncated, and 50 data points at both ends were discarded. The optimal parameters for $\boldsymbol{y_1}$ (eSNR = 37.065 dB, RMSE = 0.863) are the decomposition level j = 7, maximum Laurent polynomial degree D = 2, and the coefficients of Laurent polynomial are [0.314, −0.1, −0.189, −0.155], which means that the Laurent polynomial used in the ELS is $f(z) = 0.314z^2 - 0.1z - 0.189 - 0.155z^{-1}$; the optimal parameters for $\boldsymbol{y_2}$ (eSNR = 31.381 dB, RMSE = 1.66) are j = 8, D = 2, and the Laurent polynomial coefficients are [0.476, −0.013, −0.248, −0.371]; the optimal parameters for $\boldsymbol{y}_3$ (eSNR = 28.026 dB, RMSE = 2.438) are j = 9, D = −1, and the Laurent polynomial coefficients are [0.641, −0.338, −0.061, 0.032]. The denoising results of the three simulations are shown in Figure 6, where cyan line represents the original spectrum and red line represents the denoised spectrum. It can be clearly seen that the proposed method is able to effectively suppress random noise and, at the same time, preserve the shape of Raman peaks in simulation $\boldsymbol{y}_1$ and $\boldsymbol{y}_2$. For$\boldsymbol{y}_3$, due to the strong influence of high-level noise, the baseline of the reconstructed signal is not as smooth as those of $\boldsymbol{y}_1$ and $\boldsymbol{y}_2$, and the Raman peaks whose intensities are close to noise level (e.g., the two peaks from 1,000 to 1,050 cm^{-1}) are reconstructed to a comparatively low intensity. But the result is still acceptable.

TABLE 2 Parameters used in multi-objective genetic algorithm

Parameters	Value range and type
Decomposition level j	[1, 10], integer
Laurent polynomial length in ELS	4, integer
Laurent polynomial coefficients	[−2, 2], double
Maximum degree of Laurent polynomial	[−2, 2], integer
Population size	200
Maximum evolution generation	100
Probability of crossover	.8
Mutation function	Constraint dependent
Average change tolerance	0.0001

Note. ELS = elementary lifting step.

To prove the superior performance of the ALWT denoising method, comparison with commonly used methods, that is, first, second, and third order SG filter, and the DWT (using the base wavelet without additional lifting), was made. The window size of the SG filters was chosen to make the denoising results have similar smoothness to the results of ALWT denoising algorithm. Here, we chose the window size as 53 data points. Reducing the window size will lead to insufficient suppression of noise (i.e., not comparable with the proposed method) but will better preserve the peak features. The parameters of DWT were kept the same as ALWT denoising except for the added primal lifting step. The denoising results of the three simulated Raman spectra using the above methods are illustrated in Figure 6. And the comparison of different denoising methods in terms of the two performance assessment criteria is shown in Table 3. The best performances for the simulated spectra are highlighted in bold.

As can be seen from Figure 6, to acquire comparative smoothness in the reconstructed spectra, the first, second, and third order SG filters substantially distort the Raman peaks in all three simulations. The first order SG filter has the worst performance, that is, the peak heights are strongly affected due to the averaging process. The second and third order SG filters perform slightly better, but the four peaks in the range from 1,200 to 1,400 cm^{-1} are smoothed into two peaks. This effect can be reduced by shortening the window size but may result in insufficient noise reduction. Although ALWT and DWT have similar

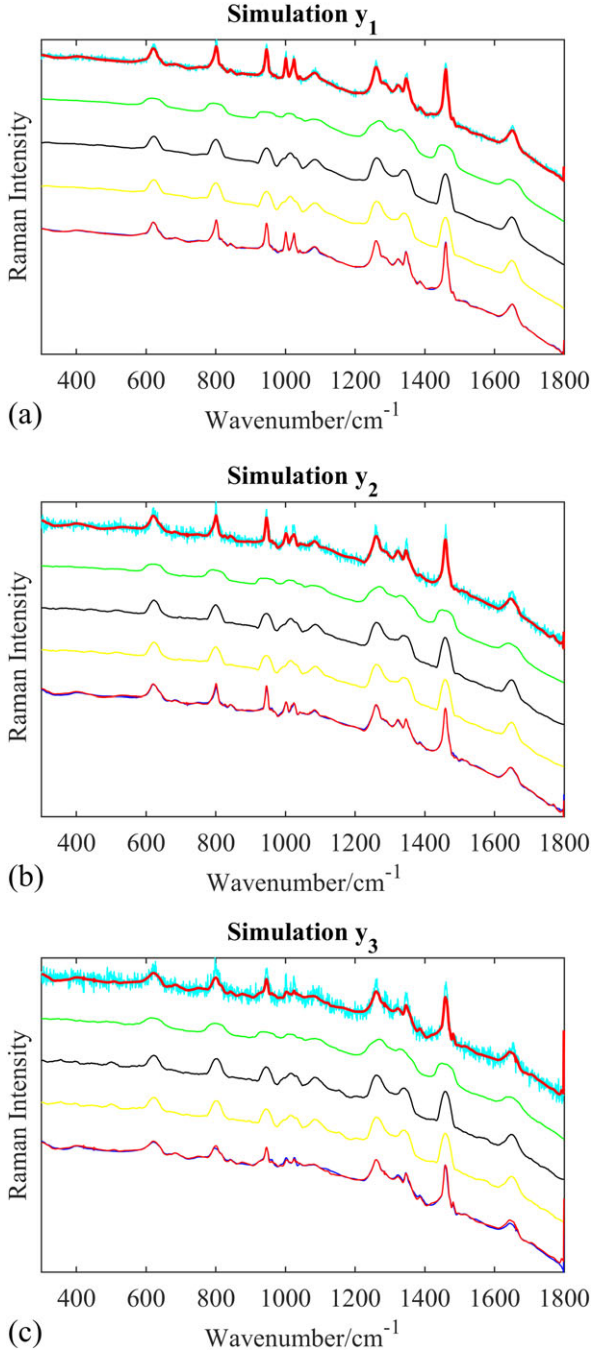

FIGURE 6 Denoising result comparison of simulated spectra between adaptive lifting wavelet transform (ALWT) denoising algorithm and first, second, and third order Savitzky–Golay (SG) filter, and discrete wavelet transform (DWT) without additional lifting (lines are offset for visualization). (a) Simulation $\mathbf{y_1}$ with 10% noise level (compared with the lowest Raman peak); (b) simulation $\mathbf{y_2}$ with 20% noise level; (c) simulation $\mathbf{y_3}$ with 30% noise level. Legends of lines: cyan line—original signal, red line—result of ALWT denoising algorithm, green line—first order SG filter, blue line—second order SG filter, yellow line—third order SG filter, and black line—DWT (base wavelet without additional lifting). ALWT and DWT denoising results are placed together for comparison (bottom lines in each subplot) [Colour figure can be viewed at wileyonlinelibrary.com]

TABLE 3 Denoising results comparison using above mentioned methods on simulated spectra

	Spectrum y_1		Spectrum y_2		Spectrum y_3	
	eSNR (dB)	RMSE	eSNR (dB)	RMSE	eSNR (dB)	RMSE
Proposed method	**37.07**	**0.86**	**31.38**	**1.66**	**28.03**	**2.44**
First order SG	28.55	2.31	27.44	2.61	26.26	3.00
Second order SG	31.98	1.55	29.90	1.97	27.87	2.50
Third order SG	31.98	1.55	29.90	1.97	27.87	2.50
DWT	36.85	0.88	31.11	1.71	27.79	2.50

Note. eSNR = estimated signal-to-noise ratio; RMSE = root mean square error; SG = Savitzky–Golay; DWT = discrete wavelet transform.

performance from visualization, ALWT has a better eSNR and RMSE value. It suppresses noise effectively while the peak heights are well retained. The evaluation of these methods using the two introduced criteria also demonstrates the effectiveness of the proposed method. From Table 3, it can be recognized that ALWT denoising has the highest eSNRs and the lowest RMSEs in all the three simulations. The performance of DWT ranks second. The second and third order SG filters have almost the same performance, whereas the first order SG filter has the poorest performance. These results indicate that the ALWT denoising algorithm is able to effectively deal with random noise (even with a considerably high-level noise) presented in Raman spectra.

4.2 | Experimental spectra

The ALWT denoising algorithm was also applied to a set of Raman spectra taken from swine fatty tissue. After performing ALWT denoising, the spectra were truncated to the range of 560 to 3,400 cm^{-1}. The three original spectra and denoising results using different methods mentioned above are shown in Figure 7. The window size of SG filters was set to 35 data points to ensure a comparative smoothness of resulting spectra. The parameters used in the GA searching process are the same as presented in Table 2.

After performing the multi-objective GA searching, the optimal parameters for the three real spectra were found. For $\mathbf{s_1}$ (90-mW laser power), the decomposition level j = 7, maximum Laurent polynomial degree D = 0, and the coefficients of Laurent polynomial are [−0.494, 0.05, −0.15, 0.364]; for $\mathbf{s_2}$ (60-mW laser power), j = 8, D = 0, and the coefficients of Laurent polynomial are [−0.768, −0.163, −0.297, 0.308]; for $\mathbf{s_3}$ (30-mW laser

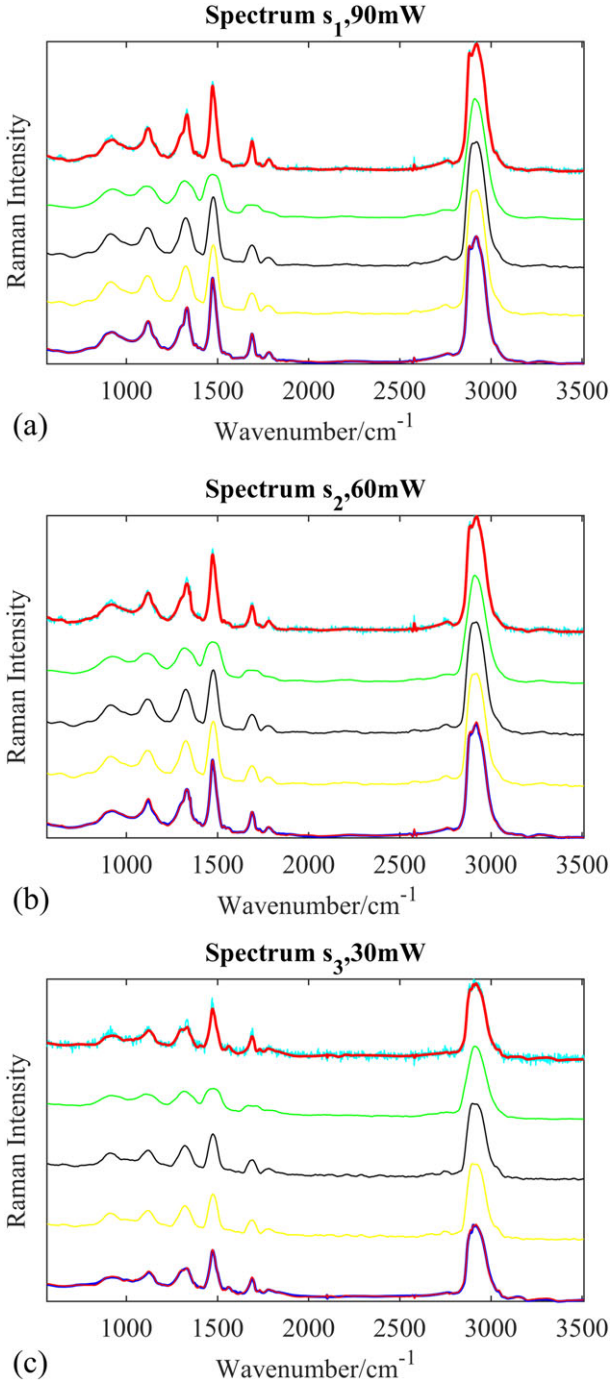

FIGURE 7 Denoising result comparison of Raman spectra of swine fatty tissue between adaptive lifting wavelet transform (ALWT) denoising algorithm and first, second, and third order Savitzky–Golay (SG) filter, and discrete wavelet transform (DWT) without additional lifting (lines are offset for visualization). (a) $\mathbf{s_1}$, 90-mW laser power; (b) $\mathbf{s_2}$, 60-mW laser power; (c) $\mathbf{s_3}$, 30-mW laser power. Legends of lines: cyan line—original signal, red line—result of ALWT denoising algorithm, green line—first order SG filter, blue line—second order SG filter, yellow line—third order SG filter, and black line—DWT (base wavelet without additional lifting). ALWT and DWT denoising results are placed together for comparison (bottom lines in each subplot) [Colour figure can be viewed at wileyonlinelibrary.com]

power), j = 7, D = 1, and the coefficients of Laurent polynomial are [0.229, −0.566, −0.24, −0.279]. Simply from visual inspection, it can be observed that the proposed method shows great effectiveness in suppressing random noise while preserving the informative Raman peaks in real spectra. The results of SG filters show different levels distortions of Raman peaks throughout the whole range due to long window size to suppress noise.

The results in terms of the two evaluation criteria are given in Table 4. The ALWT denoising algorithm has the best performance (highlighted in the table) as expected. It has the highest eSNR values and the lowest RMSEs in all experimental spectra. These results are consistent with those of simulated spectra and validate the noise reduction potential of the proposed method in real Raman spectra. Compared with DWT, with the primal ELS added to the lifting scheme of base wavelet, ALWT denoising is

TABLE 4 Denoising results comparison using above mentioned methods on real spectra

	Spectrum s_1		Spectrum s_2		Spectrum s_3	
	eSNR (dB)	RMSE	eSNR (dB)	RMSE	eSNR (dB)	RMSE
Proposed method	**27.58**	**31.20**	**25.25**	**28.49**	**16.94**	**35.68**
First order SG	15.76	118.64	18.61	60.39	13.06	54.99
Second order SG	22.55	55.97	24.87	29.95	16.90	36.75
Third order SG	22.55	55.97	24.87	29.95	16.90	36.75
DWT	27.32	32.13	24.69	30.19	16.56	36.99

Note. eSNR = estimated signal-to-noise ratio; RMSE = root mean square error; SG = Savitzky–Golay; DWT = discrete wavelet transform.

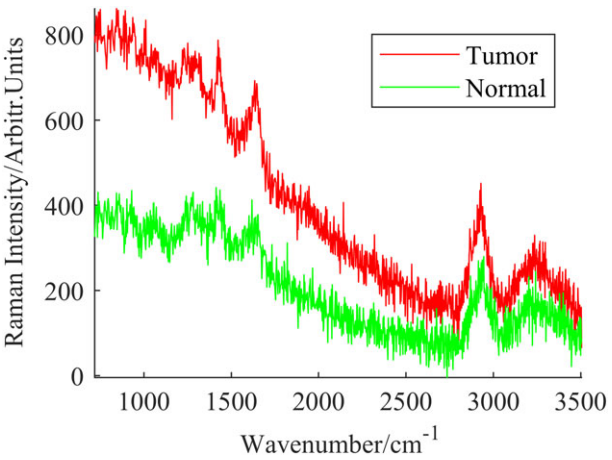

FIGURE 8 Example spectra within the bladder tissue dataset [Colour figure can be viewed at wileyonlinelibrary.com]

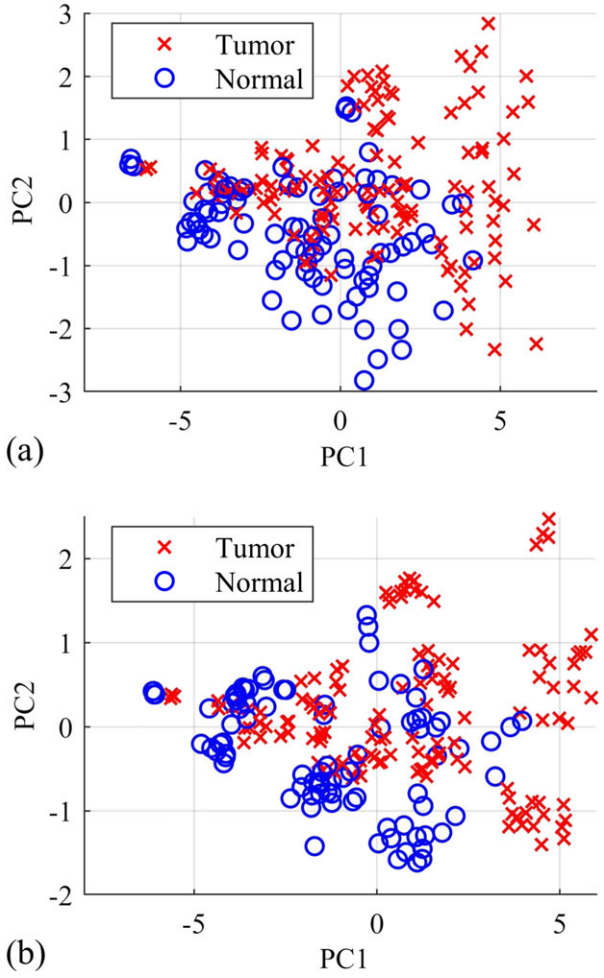

FIGURE 9 Principal component analysis score plots: (a) data denoised by discrete wavelet transform (without additional lifting); (b) data denoised by adaptive lifting wavelet transform.
PC = principal component [Colour figure can be viewed at wileyonlinelibrary.com]

adaptive to data under investigation and suppresses noise more efficiently.

4.3 | Classification dataset

A bladder tissue spectral dataset with high-noise level was selected to demonstrate the performance of ALWT denoising on a classification problem. Example spectra of bladder tumor tissue and normal bladder tissue are shown in Figure 8. The above mentioned noise reduction methods were first applied on the dataset, and then, the same preprocessing procedures described in Section 3.3 were applied. PCA-LDA models were trained and validated with 10-fold cross-validation.

Consistent with previous results on simulated and experimental spectra, the PCA-LDA model using ALWT denoising has the highest overall prediction accuracy (82.1%). The prediction accuracies using first, second, and third order SG filters, and DWT without additional lifting are 71.4%, 70%, 72.3%, and 74.1%, respectively. As expected, ALWT and DWT have a better performance over SG filters. The PCA score plots of ALWT and DWT denoised data are provided in Figure 9. A slightly better clustering of bladder tissue pathologies can be observed in the score plot of ALWT denoising compared with DWT denoising. This can be attributed to ELS of ALWT denoising, which create more suitable wavelet filters from the base wavelet.

ALWT denoising is an adaptive denoising method. Due to the procedure of GA searching, the computing time is much longer than other methods, which used fixed parameter settings. Besides, the length of input vector of GA searching and its searching range can significantly influence the computing time. Although the computing time may be longer, its performance in dealing with dataset with high-level noise can be much better. Thus, the selection between ALWT and other noise reduction methods depends on the data under investigation and the result that one expect.

5 | CONCLUSION

In this paper, we propose an ALWT denoising method for random noise suppression in Raman spectra. Compared with DWT, ALWT allows users to develop desired wavelet lifting scheme that suits the spectral data at hand from a chosen base wavelet. The newly developed lifting scheme is adaptive to the characteristics of the Raman spectral under investigation. The proposed method was tested by a set of simulated spectra with various noise level, a set of experimental Raman spectra taken from swine fatty tissue, and a classification dataset. Its performance was then compared with commonly used denoising methods in Raman spectroscopy. The results show that the ALWT denoising algorithm has the optimal performance among these methods. This algorithm is also simple to apply, which makes it a reliable tool in the preprocessing procedure within Raman data analysis. A point need to be noticed is that this method relies on GA searching. A better result is expected with a more suitable parameter searching range. Fast algorithm in improving the calculation speed of ALWT denoising will be studied in the future.

ORCID

Hao Chen http://orcid.org/0000-0003-1762-4672
Weiliang Xu http://orcid.org/0000-0002-1960-0992

REFERENCES

[1] D. I. Ellis, R. Goodacre, *Analyst* **2006**, *8*, 875.

[2] C. A. Lieber, A. Mahadevan-Jansen, *Appl. Spectrosc.* **2003**, *11*, 1363.

[3] J. Zhao, H. Lui, D. I. McLean, H. Zeng, *Appl. Spectrosc.* **2007**, *11*, 1225.

[4] Z. Zhang, S. Chen, Y. Liang, Z. Liu, Q. Zhang, L. Ding, F. Ye, H. Zhou, *J. Raman Spectrosc.* **2010**, *6*, 659.

[5] Z. Zhang, S. Chen, Y. Liang, *Analyst* **2010**, *5*, 1138.

[6] S. Baek, A. Park, J. Kim, A. Shen, J. Hu, *Chemom. Intell. Lab. Syst.* **2009**, *1*, 24.

[7] Y. Xie, L. Yang, X. Sun, D. Wu, Q. Chen, Y. Zeng, G. Liu, *Spectrochim. Acta, Part a* **2016**, *161*, 58.

[8] A. Savitzky, M. J. Golay, *Anal. Chem.* **1964**, *8*, 1627.

[9] F. Ehrentreich, L. Sümmchen, *Anal. Chem.* **2001**, *17*, 4364.

[10] J. Li, L. Choo-Smith, Z. Tang, M. G. Sowa, *J. Raman Spectrosc.* **2011**, *42*(4), 580.

[11] P. M. Ramos, I. Ruisanchez, *J. Raman Spectrosc.* **2005**, *9*, 848.

[12] C. J. Coelho, R. K. H. Galvão, M. C. U. Araujo, M. F. Pimentel, E. C. da Silva, *Chemom. Intell. Lab. Syst.* **2003**, *2*, 205.

[13] D. Chen, Z. Chen, E. Grant, *Anal. Bioanal. Chem.* **2011**, *2*, 625.

[14] W. Sweldens, *SIAM J. Math. Anal.* **1998**, *2*, 511.

[15] I. Daubechies, W. Sweldens, *J. Fourier Anal. Appl.* **1998**, *3*, 247.

[16] D. L. Donoho, *IEEE Trans. Inf. Theory* **1995**, *3*, 613.

How to cite this article: Chen H, Xu W, Broderick N, Han J. An adaptive denoising method for Raman spectroscopy based on lifting wavelet transform. *J Raman Spectrosc*. 2018;49:1529–1539. https://doi.org/10.1002/jrs.5399